Bias-hardened CMB lensing with polarization

Namikawa, T.; Takahashi, R.

Monthly Notices of the ROYAL ASTRONOMICAL SOCIETY
MNRAS **438,** 1507–1517 (2014) doi:10.1093/mnras/stt2290
Advance Access publication 2013 December 22

Bias-hardened CMB lensing with polarization

Toshiya Namikawa[1]★ and Ryuichi Takahashi[2]

[1]*Yukawa Institute for Theoretical Physics, Kyoto University, Kyoto 606-8502, Japan*
[2]*Faculty of Science and Technology, Hirosaki University, 3 bunkyo-cho, Hirosaki, Aomori, 036-8561, Japan*

Accepted 2013 November 25. Received 2013 November 15; in original form 2013 October 16

ABSTRACT

Polarization data will soon provide the best method for measuring the CMB lensing potential, although these data are potentially sensitive to several instrumental effects, including beam asymmetry, polarization angle uncertainties and sky coverage, as well as analysis choices, such as masking. We derive bias-hardened lensing estimators to mitigate these effects, at the expense of larger reconstruction noise, and we test them numerically on simulated data. We find that the mean-field bias from masking is significant for the *EE* quadratic lensing estimator. On the one hand, the bias-hardened estimator combined with filtering techniques can mitigate the mean field. On the other hand, the *EB* estimator does not significantly suffer from the mean field due to the point source masks and survey window function. However, the contamination from beam asymmetry and polarization angle uncertainties can generate mean-field biases for the *EB* estimator. These can also be mitigated using bias-hardened estimators, with at most a factor of ∼3 degradation of noise level compared to the conventional approach.

Key words: gravitational lensing: weak – cosmic background radiation – cosmology: observations.

1 INTRODUCTION

On arcminute scales, the cosmic microwave background (CMB) temperature and polarization anisotropies are distorted by gravitational lensing. For the past several years, CMB observations have been used to make increasingly precise measurements of this effect, with both cross-correlations between the CMB and large-scale structure [Smith, Zahn & Dore 2007; Hirata et al. 2008; Bleem et al. 2012; Sherwin et al. 2012; Ade et al. (Planck Collaboration) 2013c; Geach et al. 2013; Hanson et al. 2013; Holder et al. 2013] and the CMB maps alone [Das et al. 2011, 2013; van Engelen et al. 2012; Ade et al. (Planck Collaboration) 2013b; Hanson et al. 2013].

These lensing measurements are already being used to constrain cosmology [e.g. Sherwin et al. 2011; van Engelen et al. 2012; Ade et al. (Planck Collaboration) 2013a; Battye & Moss 2013; Namikawa, Yamauchi & Taruya 2013b; Wilkinson, Lesgourgues & Boehm 2013]. Future measurements are expected to quantify the sum of neutrino masses (see Namikawa, Saito & Taruya 2010; Joudaki & Kaplinghat 2012; Abazajian et al. 2013, and references therein), and to provide even tighter constraints on cosmic strings (e.g. Namikawa, Yamauchi & Taruya 2012; Yamauchi, Namikawa & Taruya 2012, 2013), primordial non-Gaussianity (e.g. Jeong, Komatsu & Jain 2009; Takeuchi, Ichiki & Matsubara 2012) and other fundamental physics. Lensing potential estimates should also be important for delensing (Kesden, Cooray & Kamionkowski 2002; Knox & Song 2002) to detect inflationary gravitational waves at $\ell > 10$ if the tensor-to-scalar ratio is less than $r \sim 0.01$.

Given an observed CMB, estimators to reconstruct the lensing potential have been derived by several authors (e.g. Seljak & Zaldarriaga 1999; Zaldarriaga & Seljak 1999; Hu & Okamoto 2002; Hirata & Seljak 2003; Okamoto & Hu 2003; Namikawa et al. 2012). These estimators all utilize the fact that a fixed lensing potential introduces statistical anisotropy into the observed CMB, in the form of a correlation between the CMB temperature/polarization anisotropies and their gradients. With a large number of observed CMB modes, this correlation can be used to form estimates of the lensing potential. The power spectrum of the lensing potential, which is of more interest for cosmological parameter constraints, can then be estimated from the power spectrum of these estimates (which probes the non-Gaussian four-point function of the lensed CMB). For CMB observations with noise levels below 5 μK arcmin, *B*-mode polarization is a particularly powerful probe of lensing because it is believed to be dominated by the lensing contribution on scales $\ell \gtrsim 100$.

For realistic CMB observations, there are so-called mean-field biases for the standard minimum-variance quadratic lensing estimators because of non-lensing sources of statistical anisotropy, such as masking, inhomogeneous map noise, beam asymmetry, or spatially varying errors in the detector polarization angles. With a perfect statistical understanding of the unlensed CMB and the instrument used to observe it, these biases can be corrected for, but given the imperfections in our understanding of these quantities it can be useful to design estimators that are less sensitive to them.

★ E-mail: namikawa@utap.phys.s.u-tokyo.ac.jp

Approaches have been proposed in the literature to mitigate some of the mean-field biases. For example, the mean fields from masking in temperature have been studied by several authors, with approaches including simply avoiding mask boundaries (Hirata et al. 2008; Carvalho & Tereno 2011), or using inpainting/apodization (Perotto et al. 2010; Plaszczynski et al. 2012; Benoit-Levy et al. 2013) to smooth them. These techniques could also be utilized for polarization, in conjunction with pure estimators for E and B modes (Smith 2006; Smith & Zaldarriaga 2007). For temperature, the mean-field bias from an inhomogeneous map noise has also been studied by Hanson, Rocha & Gorski (2009).

In this paper, we extend the bias-hardened estimators proposed in our previous work (Namikawa, Hanson & Takahashi 2013a) to the case of lensing reconstruction with polarization, constructing lensing estimators that can have significantly smaller mean-field biases than the standard minimum-variance estimators, with minimal loss of signal-to-noise.

This paper is organized as follows. In Section 2, we briefly summarize the quadratic estimators for the lensing potential using CMB temperature and polarization. In Section 3, we discuss several possible mean-field biases, which must be corrected for, and then we construct the corresponding bias-hardened estimators. In Section 4, we demonstrate the usefulness of bias-hardened estimators using numerical simulations. In Section 5, we summarize our results.

Finally, we note that when estimating the power spectrum of the lensing potential, there is an additional worrisome bias, the reconstruction noise bias, which must be accounted for. This bias is analogous to shape-noise in galaxy weak-lensing measurements. In principle, it can be avoided by forming independent lensing estimates from subsets of the observed sky modes, for example, using an odd/even parity split (Hu 2001) or the in/out Fourier split (Sherwin & Das 2010). However, there is usually a substantial loss of signal-to-noise associated with such splits. This bias is less of an issue in polarization than in temperature, because it falls with the instrumental noise level for estimates that utilize B-mode polarization, and it can also be avoided using cross-spectra between different lensing estimates. In Appendix A, we present a polarized derivation of the optimal trispectrum-estimator approach to correcting for this bias, also extending our discussion of this approach for the temperature case in (Namikawa et al. 2013a).

2 QUADRATIC LENSING RECONSTRUCTION FROM CMB MAPS

2.1 Lensing effect on CMB anisotropies

The distortion effect of lensing on the primary temperature and polarization anisotropies is expressed by a remapping of the primary anisotropies. Denoting the primary CMB anisotropies at position $\hat{\boldsymbol{n}} = (\theta, \varphi)$ on the last scattering surface as $\Xi^{(s)}(\hat{\boldsymbol{n}})$, where $s = 0$ denotes the temperature, $\Xi^{(0)} = \Theta$, while $s = \pm 2$ are the spin-2 combination of the Stokes parameter, $\Xi^{(\pm 2)} = Q \pm \mathrm{i}U \equiv P^{\pm}$, the lensed anisotropies in a direction $\hat{\boldsymbol{n}}$ are given by (e.g. Lewis & Challinor 2006)

$$\widetilde{\Xi}^{(s)}(\hat{\boldsymbol{n}}) = \Xi^{(s)}(\hat{\boldsymbol{n}} + \boldsymbol{d}(\hat{\boldsymbol{n}})) = \Xi^{(s)}(\hat{\boldsymbol{n}}) + d^a(\hat{\boldsymbol{n}})\partial_a \Xi^{(s)}(\hat{\boldsymbol{n}}) + \mathcal{O}(|\boldsymbol{d}|^2). \quad (1)$$

The two-dimensional vector, $d^a(\hat{\boldsymbol{n}})$ $(a = \theta, \varphi)$, is the deflection angle, and, in terms of parity symmetry, we can decompose it into two terms, known as gradient (even parity) and curl (odd parity) modes (e.g. Hirata & Seljak 2003; Cooray, Kamionkowski & Caldwell 2005; Namikawa et al. 2012):

$$d^a(\hat{\boldsymbol{n}}) = \partial^a \phi(\hat{\boldsymbol{n}}) + \epsilon^{ab}\partial_b \varpi(\hat{\boldsymbol{n}}) = \sum_{x=\phi,\varpi} c_x^{ab}\partial_b x(\hat{\boldsymbol{n}}), \quad (2)$$

where c_ϕ^{ab} is the Kronecker delta and $c_\varpi^{ab} = \epsilon^{ab}$ is the two-dimensional Levi–Chivita symbol.

2.2 Estimator for lensing fields

The temperature anisotropies are distorted by lensing as (e.g. Hu & Okamoto 2002)[1]

$$\widetilde{\Theta}_\ell = \Theta_\ell - \sum_{x=\phi,\varpi}\int \frac{\mathrm{d}^2\boldsymbol{L}}{(2\pi)^2} c_x^{ab} L_a(\ell_b - L_b)\phi_L \Theta_{\ell-L}. \quad (3)$$

However, for polarization, we usually use the rotationally invariant combination, that is, the E- and B-mode polarizations, instead of the spin-2 quantity (e.g. Hu & Okamoto 2002):

$$E_\ell \pm \mathrm{i}B_\ell = -\int \mathrm{d}^2\hat{\boldsymbol{n}} \mathrm{e}^{-\mathrm{i}\hat{\boldsymbol{n}}\cdot\boldsymbol{\ell}} P^{\pm}(\hat{\boldsymbol{n}}) \mathrm{e}^{\mp 2\mathrm{i}\varphi_\ell}, \quad (4)$$

where φ_ℓ is the angle of $\boldsymbol{\ell}$ measured from the x-axis. With the deflection angle given in equation (2), the lensed E and B modes are given by (e.g. Hu & Okamoto 2002; Cooray et al. 2005; Namikawa et al. 2012)

$$\widetilde{E}_\ell = E_\ell - \int \frac{\mathrm{d}^2\boldsymbol{L}}{(2\pi)^2} (L^a L'_a \phi_L + \epsilon^{ab} L_a L'_b \varpi_\ell) \times (E_{L'} \cos 2\varphi_{L',\ell} - B_{L'} \sin 2\varphi_{L',\ell}), \quad (5)$$

$$\widetilde{B}_\ell = B_\ell - \int \frac{\mathrm{d}^2\boldsymbol{L}}{(2\pi)^2} (L^a L'_a \phi_L + \epsilon^{ab} L_a L'_b \varpi_\ell) \times (B_{L'} \cos 2\varphi_{L',\ell} + E_{L'} \sin 2\varphi_{L',\ell}), \quad (6)$$

with $\boldsymbol{L}' = \boldsymbol{\ell} - \boldsymbol{L}$ and $\varphi_{\ell_1,\ell_2} \equiv \varphi_{\ell_1} - \varphi_{\ell_2}$.

Denoting X and Y as Θ, E or B, the off-diagonal covariance includes the gradient and curl modes of deflections as

$$\langle \widetilde{X}_L \widetilde{Y}_{L'} \rangle_{\mathrm{CMB}} = f_{\ell,L}^{x,(XY)} x_\ell, \quad (7)$$

where $\langle \cdots \rangle_{\mathrm{CMB}}$ denotes the ensemble average over unlensed Θ, E or B, with a fixed realization of the gradient and curl modes, and we ignore the higher-order terms of lensing fields. The weight functions for gradient and curl modes are summarized in Table 1 (Hu & Okamoto 2002; Cooray et al. 2005; Namikawa et al. 2012). Note that, to mitigate the higher-order biases (Hanson et al. 2011), the lensed power spectrum is used rather than the unlensed one (Lewis, Challinor & Hanson 2011; Anderes 2013). With a quadratic combination of X and Y fluctuations, the lensing estimators are then formed as (e.g. Hu & Okamoto 2002)

$$\widehat{x}_\ell^{(XY)} = \frac{1}{2} A_\ell^{x,(XY)} \int \frac{\mathrm{d}^2\boldsymbol{L}}{(2\pi)^2} g_{\ell,L}^{x,(XY)} \overline{X}_L \overline{Y}_{L'}, \quad (8)$$

[1] Our definitions of the Fourier transform and its inverse for arbitrary quantity $X(\hat{\boldsymbol{n}})$ on a map are

$$X_\ell = \int \mathrm{d}^2\hat{\boldsymbol{n}} \mathrm{e}^{-\mathrm{i}\hat{\boldsymbol{n}}\cdot\boldsymbol{\ell}} X(\hat{\boldsymbol{n}}),$$

$$X(\hat{\boldsymbol{n}}) = \int \frac{\mathrm{d}^2\boldsymbol{\ell}}{(2\pi)^2} \mathrm{e}^{\mathrm{i}\boldsymbol{\ell}\cdot\hat{\boldsymbol{n}}} X_\ell.$$

These are the same as Hu & Okamoto (2002) but different from, for example, Lewis & Challinor (2006).

Table 1. The weight functions for lensing potentials, $f^{x,(XY)}_{\boldsymbol{\ell},\boldsymbol{L}}$. Note that $\boldsymbol{L}' = \boldsymbol{\ell} - \boldsymbol{L}$.

Lensing	
$\Theta\Theta$	$c_x^{ab}\left(\ell_a L_b \widetilde{C}^{\Theta\Theta}_L + \ell_a L'_b \widetilde{C}^{\Theta\Theta}_{L'}\right)$
ΘE	$c_x^{ab}\left(\ell_a L_b \widetilde{C}^{\Theta E}_L \cos 2\varphi_{\boldsymbol{L},\boldsymbol{L}'} + \ell_a L'_b \widetilde{C}^{\Theta E}_{L'}\right)$
ΘB	$c_x^{ab}\ell_a L_b \widetilde{C}^{\Theta E}_L \sin 2\varphi_{\boldsymbol{L},\boldsymbol{L}'}$
EE	$c_x^{ab}\left(\ell_a L_b \widetilde{C}^{EE}_L + \ell_a L'_b \widetilde{C}^{EE}_{L'}\right) \cos 2\varphi_{\boldsymbol{L},\boldsymbol{L}'}$
EB	$c_x^{ab}\left(\ell_a L_b \widetilde{C}^{EE}_L + \ell_a L'_b \widetilde{C}^{BB}_{L'}\right) \sin 2\varphi_{\boldsymbol{L},\boldsymbol{L}'}$
BB	$c_x^{ab}\left(\ell_a L_b \widetilde{C}^{BB}_L + \ell_a L'_b \widetilde{C}^{BB}_{L'}\right) \cos 2\varphi_{\boldsymbol{L},\boldsymbol{L}'}$

where, with the ratio of power spectra, $r^{XY}_L = \widehat{C}^{XY}_L / \widehat{C}^{XX}_L$, we define[2]

$$g^{x,(XY)}_{\boldsymbol{\ell},\boldsymbol{L}} = 2\frac{\left[f^{x,(XY)}_{\boldsymbol{\ell},\boldsymbol{L}}\right]^* - r^{XY}_L r^{YX}_{L'}\left[f^{x,(XY)}_{\boldsymbol{\ell},\boldsymbol{L}'}\right]^*}{1 - r^{XY}_L r^{XY}_{L'} r^{YX}_L r^{YX}_{L'}}, \tag{9}$$

$$A^{x,(XY)}_\ell = \left[\int \frac{\mathrm{d}^2\boldsymbol{L}}{(2\pi)^2}\frac{g^{x,(XY)}_{\boldsymbol{\ell},\boldsymbol{L}} f^{x,(XY)}_{\boldsymbol{\ell},\boldsymbol{L}}}{2\widehat{C}^{XX}_L \widehat{C}^{YY}_{L'}}\right]^{-1}. \tag{10}$$

The inverse-variance filtered Fourier modes are given by

$$\overline{X}_{\boldsymbol{\ell}} = \frac{\widehat{X}_{\boldsymbol{\ell}}}{\widehat{C}^{XX}_\ell}. \tag{11}$$

For the cosmic variance case, the estimated power spectrum reduces to the lensed power spectrum.

3 BIAS-HARDENED LENSING ESTIMATORS

There are many effects that can generate mode-coupling between observed Θ, E and B modes, leading to mean-field biases for the conventional lensing estimators. In the following, we compute the non-lensing statistical anisotropy due to masking, inhomogeneous noise (and/or unresolved point sources) and polarization angle (or scan strategy) systematics in the presence of beam asymmetry. Then, in order to mitigate the mean-field biases from these systematics, we construct bias-hardened estimator analogous to those of our previous work (Namikawa et al. 2013a).

3.1 Non-lensing sources in the off-diagonal covariance

3.1.1 Masking

Let us first consider the modification due to a window function, $M(\hat{\boldsymbol{n}})$, which is defined to be zero for an unmasked region and otherwise unity:

$$\widehat{\Theta}(\hat{\boldsymbol{n}}) = [1 - M(\hat{\boldsymbol{n}})]\,\widetilde{\Theta}(\hat{\boldsymbol{n}}), \tag{12}$$

$$\widehat{P}^{\pm}(\hat{\boldsymbol{n}}) = [1 - M(\hat{\boldsymbol{n}})]\,\widetilde{P}^{\pm}(\hat{\boldsymbol{n}}). \tag{13}$$

Such masking mixes E and B modes, leading to mode-coupling in temperature and polarization as

$$\widehat{\Theta}_{\boldsymbol{\ell}} = \widetilde{\Theta}_{\boldsymbol{\ell}} - \int \frac{\mathrm{d}^2\boldsymbol{L}}{(2\pi)^2} M_{\boldsymbol{L}} \widetilde{\Theta}_{\boldsymbol{L}'}, \tag{14}$$

[2] Note, here, that the normalization, $A^{x,(XY)}_{\boldsymbol{\ell}}$, is independent of the direction of $\boldsymbol{\ell}$, so we write the normalization as $A^{x,(XY)}_\ell$.

Table 2. The weight functions for masking, $f^{M,(XY)}_{\boldsymbol{\ell},\boldsymbol{L}}$. Note that $\boldsymbol{L}' = \boldsymbol{\ell} - \boldsymbol{L}$.

Masking	
$\Theta\Theta$	$-\widetilde{C}^{\Theta\Theta}_L - \widetilde{C}^{\Theta\Theta}_{L'}$
ΘE	$-\widetilde{C}^{\Theta E}_L \cos 2\varphi_{\boldsymbol{L},\boldsymbol{L}'} - \widetilde{C}^{\Theta E}_{L'}$
ΘB	$-\widetilde{C}^{\Theta E}_L \sin 2\varphi_{\boldsymbol{L},\boldsymbol{L}'}$
EE	$-\left(\widetilde{C}^{EE}_L + \widetilde{C}^{EE}_{L'}\right) \cos\varphi_{\boldsymbol{L},\boldsymbol{L}'}$
EB	$-\left(\widetilde{C}^{EE}_L + \widetilde{C}^{BB}_{L'}\right) \sin\varphi_{\boldsymbol{L},\boldsymbol{L}'}$
BB	$-\left(\widetilde{C}^{BB}_L + \widetilde{C}^{BB}_{L'}\right) \cos\varphi_{\boldsymbol{L},\boldsymbol{L}'}$

$$\widehat{E}_{\boldsymbol{\ell}} = \widetilde{E}_{\boldsymbol{\ell}} - \int \frac{\mathrm{d}^2\boldsymbol{L}}{(2\pi)^2} M_{\boldsymbol{L}} \left(\widetilde{E}_{\boldsymbol{L}'} \cos\varphi_{\boldsymbol{L}',\boldsymbol{L}} - \widetilde{B}_{\boldsymbol{L}'} \sin\varphi_{\boldsymbol{L}',\boldsymbol{L}}\right), \tag{15}$$

$$\widehat{B}_{\boldsymbol{\ell}} = \widetilde{B}_{\boldsymbol{\ell}} - \int \frac{\mathrm{d}^2\boldsymbol{L}}{(2\pi)^2} M_{\boldsymbol{L}} \left(\widetilde{B}_{\boldsymbol{L}'} \cos\varphi_{\boldsymbol{L}',\boldsymbol{L}} + \widetilde{E}_{\boldsymbol{L}'} \sin\varphi_{\boldsymbol{L}',\boldsymbol{L}}\right). \tag{16}$$

With the above equations, the resultant off-diagonal covariance can be written as

$$\langle \widehat{X}_{\boldsymbol{L}} \widehat{Y}_{\boldsymbol{L}'} \rangle = M_{\boldsymbol{\ell}} f^{M,(XY)}_{\boldsymbol{\ell},\boldsymbol{L}} + \mathcal{O}(M^2), \tag{17}$$

where $\langle \cdots \rangle$ denotes the usual ensemble average, and the weight functions are summarized in Table 2. Equation (17) implies that the resultant lensing estimator has mean-field bias due to the mask field, $M_{\boldsymbol{\ell}}$.

3.1.2 Inhomogeneous noise/unresolved point-source

Next, let us consider the modification because of the addition of arbitrary sky signals, $n^T(\hat{\boldsymbol{n}})$, $n^Q(\hat{\boldsymbol{n}})$ and $n^U(\hat{\boldsymbol{n}})$, which are uncorrelated between pixels; this approach can be used to model, for example, residual point sources and inhomogeneous instrumental noise in temperature and polarization maps. The corresponding Θ, E and B modes are given by

$$n^\Theta_{\boldsymbol{\ell}} = \int \mathrm{d}^2\hat{\boldsymbol{n}} \mathrm{e}^{-\mathrm{i}\hat{\boldsymbol{n}}\cdot\boldsymbol{\ell}}\, n^T(\hat{\boldsymbol{n}}), \tag{18}$$

and

$$n^E_{\boldsymbol{\ell}} \pm \mathrm{i} n^B_{\boldsymbol{\ell}} = \int \mathrm{d}^2\hat{\boldsymbol{n}} \mathrm{e}^{-\mathrm{i}\hat{\boldsymbol{n}}\cdot\boldsymbol{\ell}} \left(n^Q \pm \mathrm{i} n^U\right)(\hat{\boldsymbol{n}}) \mathrm{e}^{\mp 2\mathrm{i}\varphi_{\boldsymbol{\ell}}}. \tag{19}$$

Assuming that $\langle n^X(\hat{\boldsymbol{n}}) n^Y(\hat{\boldsymbol{n}}')\rangle = S^{(XY)}(\hat{\boldsymbol{n}})\delta(\hat{\boldsymbol{n}} - \hat{\boldsymbol{n}}')$, we have

$$\begin{aligned}\left\langle n^X_{\boldsymbol{L}} n^Y_{\boldsymbol{L}'}\right\rangle &= \int \mathrm{d}^2\hat{\boldsymbol{n}} \mathrm{e}^{-\mathrm{i}\hat{\boldsymbol{n}}\cdot\boldsymbol{L}} \int \mathrm{d}^2\hat{\boldsymbol{n}}' \mathrm{e}^{-\mathrm{i}\hat{\boldsymbol{n}}'\cdot\boldsymbol{L}'} \left\langle n^X(\hat{\boldsymbol{n}}) n^Y(\hat{\boldsymbol{n}}')\right\rangle \\ &= \int \mathrm{d}^2\hat{\boldsymbol{n}} \mathrm{e}^{-\mathrm{i}\hat{\boldsymbol{n}}\cdot\boldsymbol{\ell}}\, S^{(XY)}(\hat{\boldsymbol{n}}) \equiv S^{(XY)}_{\boldsymbol{\ell}},\end{aligned} \tag{20}$$

where we use $\boldsymbol{L} + \boldsymbol{L}' = \boldsymbol{\ell}$. The off-diagonal covariance then has additional terms

$$\left\langle \widehat{X}_{\boldsymbol{L}} \widehat{Y}_{\boldsymbol{L}'} \right\rangle = \left\langle n^X_{\boldsymbol{L}} n^Y_{\boldsymbol{L}'} \right\rangle = f^{S,(XY)}_{\boldsymbol{\ell},\boldsymbol{L}} S^{(XY)}_{\boldsymbol{\ell}}. \tag{21}$$

where the weight function is $f^{S,(XY)}_{\boldsymbol{\ell},\boldsymbol{L}} = 1$.

3.1.3 Polarization angle with beam asymmetry

Instrumental effects, such as beam asymmetry and errors in the detector polarization angles, are also a potential concern for lensing

reconstruction. Here, we consider the effect of a spatial variation in the polarization angle in the presence of the ellipticity in beam shape.

Denoting CMB temperature and polarization anisotropies as $\Xi^{(0)} = \Theta$ and $\Xi^{(\pm 2)} = Q \pm \mathrm{i}U = P^{\pm}$, we assume that the beam-convolved anisotropies for the ith pixel are expressed as

$$\Xi^{(s)}(\hat{\boldsymbol{n}}_i) = \int \mathrm{d}^2\hat{\boldsymbol{n}}\ \mathcal{R}[\hat{\boldsymbol{n}}_i - \hat{\boldsymbol{n}}, \alpha(\hat{\boldsymbol{n}}_i)]\Xi^{(s)}(\hat{\boldsymbol{n}}), \tag{22}$$

where $s = 0$ (temperature) or ± 2 (polarization), and $\mathcal{R}$ denotes the beam-response function whose shape is independent of the measurements but whose orientation angle, $\alpha(\hat{\boldsymbol{n}}_i)$ (Shimon et al. 2008), is dependent on both the pixels and measurements. The beam-response function, $\mathcal{R}$, is given by

$$\mathcal{R}[\boldsymbol{r}, \alpha(\hat{\boldsymbol{n}}_i)] = \int \frac{\mathrm{d}^2\boldsymbol{L}}{(2\pi)^2}\ \mathrm{e}^{\mathrm{i}\boldsymbol{L}\cdot\boldsymbol{r}}\mathcal{R}_{\boldsymbol{L}}(\hat{\boldsymbol{n}}_i), \tag{23}$$

where the Fourier counterpart of the beam-response function is expanded as (Shimon et al. 2008)

$$\mathcal{R}_{\boldsymbol{L}}(\hat{\boldsymbol{n}}_i) = \sum_{n=-\infty}^{\infty} b_{L,n}\,\mathrm{e}^{-\mathrm{i}n\alpha(\hat{\boldsymbol{n}}_i)}\mathrm{e}^{\mathrm{i}n\varphi_L}. \tag{24}$$

Here, by denoting the Bessel function as J_n, the coefficients are given by

$$b_{L,n} = \mathrm{i}^n \int \mathrm{d}r\ rJ_n(Lr)\int \frac{\mathrm{d}\varphi_r}{2\pi}\,\mathcal{R}(\boldsymbol{r}, 0)\mathrm{e}^{-\mathrm{i}n\varphi_r}. \tag{25}$$

Note that $b_{L,-n} = b_{L,n}$, and if the shape of beam function, $R(\boldsymbol{r}, 0)$, does not depend on the angle, φ_r (e.g. a circular Gaussian beam), the coefficients are non-zero only when $n = 0$. The beam-convolved anisotropies are then rewritten as

$$\Xi^{(s)}(\hat{\boldsymbol{n}}_i) = \mathrm{i}^s \sum_{n=-\infty}^{\infty} \mathrm{e}^{-\mathrm{i}n\alpha(\hat{\boldsymbol{n}}_i)}\int \frac{\mathrm{d}^2\boldsymbol{L}}{(2\pi)^2}\,b_{L,n}\,\Xi^{(s)}_{\boldsymbol{L}}\,\mathrm{e}^{\mathrm{i}\boldsymbol{L}\cdot\hat{\boldsymbol{n}}_i}\,\mathrm{e}^{\mathrm{i}(n+s)\varphi_L}, \tag{26}$$

where $\Xi^{(0)} = \Theta$ and $\Xi^{(\pm 2)} = E \pm \mathrm{i}B$.

For a two-beam experiment, as shown in Shimon et al. (2008), the measured temperature and polarization anisotropies are distorted by the polarization angle and the differences in beam shapes between the first and second detectors. If the anisotropies are measured several times at each pixel, the optimal estimators for temperature and polarization anisotropies are given by (Shimon et al. 2008)

$$\widehat{\Xi}^{(0)} = \left\langle \Xi^{(0)}_{+} \right\rangle_{\mathrm{pix}} + \frac{1}{2}\left\langle \Xi^{(-2)}_{-}\mathrm{e}^{2\mathrm{i}\widehat{\alpha}_t}\mathrm{e}^{-2\mathrm{i}\delta_t}\right\rangle_{\mathrm{pix}} + \frac{1}{2}\left\langle \Xi^{(+2)}_{-}\mathrm{e}^{-2\mathrm{i}\widehat{\alpha}_t}\mathrm{e}^{2\mathrm{i}\delta_t}\right\rangle_{\mathrm{pix}}, \tag{27}$$

$$\widehat{\Xi}^{(\pm 2)} = \left\langle \Xi^{(\pm 2)}_{+}\mathrm{e}^{\pm 2\mathrm{i}\delta_t}\widehat{\Psi}^{\pm}_t\right\rangle_{\mathrm{pix}} + \left\langle \Xi^{(\mp 2)}_{+}\mathrm{e}^{\mp 2\mathrm{i}\delta_t}\mathrm{e}^{\pm 4\mathrm{i}\widehat{\alpha}_t}\widehat{\Psi}^{\pm}_t\right\rangle_{\mathrm{pix}} + 2\left\langle \Xi^{(0)}_{-}\mathrm{e}^{\pm 2\mathrm{i}\widehat{\alpha}_t}\widehat{\Psi}^{\pm}_t\right\rangle_{\mathrm{pix}}, \tag{28}$$

where the arguments, $\hat{\boldsymbol{n}}_i$, are dropped. The bracket, $\langle\cdots\rangle_{\mathrm{pix}}$, denotes the average over all measurements in each pixel, and $\widehat{\alpha}_t$ is the estimated polarization angle for tth measurement at each pixel, which has small polarization angle error $\delta_t \equiv \widehat{\alpha}_t - \alpha_t$. We also define

$$\widehat{\Psi}^{\pm 1}_t = \frac{1 - \mathrm{e}^{\mp 4\mathrm{i}\widehat{\alpha}_t}\langle \mathrm{e}^{\pm 4\mathrm{i}\widehat{\alpha}_t}\rangle_{\mathrm{pix}}}{1 - \langle \mathrm{e}^{\mp 4\mathrm{i}\widehat{\alpha}_t}\rangle_{\mathrm{pix}}\langle \mathrm{e}^{\pm 4\mathrm{i}\widehat{\alpha}_t}\rangle_{\mathrm{pix}}}. \tag{29}$$

The subscripts, $+$ and $-$, in Ξ^s are the total and the difference, respectively, of anisotropies obtained from the two detectors:

$$\Xi^{(s)}_{+} = \frac{\Xi^{(s)}_1 \pm \Xi^{(s)}_2}{2}. \tag{30}$$

Note that, if the temperature and polarization anisotropies are measured only one time for each pixel, the quantities, $\widehat{\Psi}^{\pm 1}_t$, in equations (27) and (28) should be replaced with unity.

With equations (27) and (28), taking into account the polarization angle involved in $\Xi^{(s)}$, the measured temperature and polarization in Fourier space are given by

$$\widehat{X}_{\boldsymbol{\ell}} = \sum_{n=-\infty}^{\infty}\sum_{p=0,\pm 1}\sum_{Y=\Theta,E,B}\int \frac{\mathrm{d}^2\boldsymbol{L}}{(2\pi)^2} \times \mathcal{B}^{(XY)}_{L,(n,p)}\widetilde{Y}_{\boldsymbol{L}}\psi^{(n,p)}_{\boldsymbol{L}'}\,\mathrm{e}^{\mathrm{i}n\varphi_{\boldsymbol{L},\boldsymbol{L}'}}\,\mathrm{e}^{2\mathrm{i}p\varphi_{\boldsymbol{L},\boldsymbol{\ell}}}, \tag{31}$$

where $X = \Theta, E$ or B. The quantities, $\psi^{(n,p)}_{\boldsymbol{L}}$ $(p = 0, \pm 1)$, are defined as the Fourier transform of the following quantities,

$$\psi^{(n,p)}(\hat{\boldsymbol{n}}_i) = \langle \mathrm{e}^{-\mathrm{i}n\widehat{\alpha}_t(\hat{\boldsymbol{n}}_i)}\,\mathrm{e}^{\mathrm{i}(n+2p)\delta_t(\hat{\boldsymbol{n}}_i)}\widehat{\Psi}^{p}_t(\hat{\boldsymbol{n}}_i)\rangle_{\mathrm{pix}}\,\mathrm{e}^{\mathrm{i}n\varphi_{\boldsymbol{L}}}, \tag{32}$$

with $\widehat{\Psi}^0_t = 1$. Note that $\psi^{(n,p)}_{\boldsymbol{L}}$ is the spin-$(-n)$ transform of spin-$(-n)$ quantity, $\langle \mathrm{e}^{-\mathrm{i}n\widehat{\alpha}_t(\hat{\boldsymbol{n}}_i)}\widehat{\Psi}^{p}_t(\hat{\boldsymbol{n}}_i)\rangle_{\mathrm{pix}}$, in the limit of $\delta_i = 0$ for all measurements. The coefficients, $\mathcal{B}^{(ZZ')}_{L,(n,p)}$, are given by

$$\begin{aligned}
\mathcal{B}^{(\Theta\Theta)}_{L,(n,0)} &= b^{+}_{L,n}\\
\mathcal{B}^{(\Theta E)}_{L,(n,0)} &= -\frac{b^{-}_{L,n+2} + b^{-}_{L,n-2}}{2}\\
\mathcal{B}^{(\Theta B)}_{L,(n,0)} &= \mathrm{i}\frac{b^{-}_{L,n+2} - b^{-}_{L,n-2}}{2}\\
\mathcal{B}^{(E\Theta)}_{L,(n,\pm 1)} &= -b^{-}_{L,n\pm 2}\\
\mathcal{B}^{(EE)}_{L,(n,\pm 1)} &= \frac{b^{+}_{L,n} + b^{+}_{L,n\pm 4}}{2}\\
\mathcal{B}^{(EB)}_{L,(n,\pm 1)} &= \pm\mathrm{i}\frac{b^{+}_{L,n} - b^{+}_{L,n\pm 4}}{2}\\
\mathcal{B}^{(BY)}_{L,(n,\pm 1)} &= \mp\mathrm{i}\mathcal{B}^{(EY)}_{L,(n,\pm 1)},
\end{aligned} \tag{33}$$

where $b^{\pm}_{L,n}$ is the total and the difference of beam transfer functions for the two detectors:

$$b^{\pm}_{L,n} = \frac{b^{(1)}_{L,n} \pm b^{(2)}_{L,n}}{2}. \tag{34}$$

Note that, in full sky and the temperature-only case, equation (31) is consistent with Hanson, Lewis & Challinor (2010).

In Fourier space, we break $\psi^{(n,p)}_{\boldsymbol{\ell}}$ into constant and fluctuation pieces

$$\psi^{(n,p)}_{\boldsymbol{\ell}} = C^{(n,p)}\delta_{\boldsymbol{\ell}=\boldsymbol{0}} + (\psi^{(n,p)}_{\boldsymbol{\ell}})_{\mathrm{ani}}, \tag{35}$$

with the assumption that $(\psi^{(n,p)}_{\boldsymbol{\ell}})_{\mathrm{ani}}$ are small. Then, equation (31) is rewritten as

$$\widehat{X}_{\boldsymbol{\ell}} = \sum_{n=-\infty}^{\infty}\sum_{p=0,\pm 1}\sum_{Y=\Theta,E,B}\left[\mathcal{B}^{(XY)}_{\ell,(n,p)}\widetilde{Y}_{\boldsymbol{\ell}}\,\mathrm{e}^{\mathrm{i}n\varphi_{\boldsymbol{\ell}}}C^{(n,p)} + \int \frac{\mathrm{d}^2\boldsymbol{L}}{(2\pi)^2}\,\mathcal{B}^{(XY)}_{L,(n,p)}\widetilde{Y}_{\boldsymbol{L}}(\psi^{(n,p)}_{\boldsymbol{L}'})_{\mathrm{ani}}\,\mathrm{e}^{\mathrm{i}n\varphi_{\boldsymbol{L},\boldsymbol{L}'}}\,\mathrm{e}^{2\mathrm{i}p\varphi_{\boldsymbol{L},\boldsymbol{\ell}}}\right], \tag{36}$$

For realistic cases, $b^{+}_{L,n}/b^{+}_{L,0} \ll 1$ for $n \neq 0$, $b^{-}_{L,n} \ll b^{+}_{L,n}$ and $\delta_i \ll 1$. Under these approximations, the dominant term in the

Table 3. Same as Table 2, but for polarization angle, $f^{\psi^{(n,p)},(XY)}_{\ell,\boldsymbol{L}}$. For clarity, the exponential is expressed as 'exp'.

$p=0$	
$\Theta\Theta$	$\left[\mathcal{B}^{(\Theta\Theta)}_{L,(n,0)}\widetilde{C}^{\Theta\Theta}_{L}+\mathcal{B}^{(\Theta E)}_{L,(n,0)}\widetilde{C}^{\Theta E}_{L}\right]\exp(in\varphi_{-\boldsymbol{L},\boldsymbol{\ell}})+(\boldsymbol{L}\leftrightarrow\boldsymbol{L}')$
ΘE	$\left[\mathcal{B}^{(\Theta\Theta)}_{L',(n,0)}\widetilde{C}^{\Theta E}_{L'}+\mathcal{B}^{(\Theta E)}_{L',(n,0)}\widetilde{C}^{EE}_{L'}\right]\exp(in\varphi_{-\boldsymbol{L}',\boldsymbol{\ell}})$
ΘB	$\mathcal{B}^{(\Theta B)}_{L',(n,0)}\widetilde{C}^{BB}_{L'}\exp(in\varphi_{-\boldsymbol{L}',\boldsymbol{\ell}})$
EE	0
EB	0
BB	0
$p=\pm1$	
$\Theta\Theta$	0
ΘE	$\left[\mathcal{B}^{(E\Theta)}_{L,(n,p)}\widetilde{C}^{\Theta\Theta}_{L}+\mathcal{B}^{(EE)}_{L,(n,p)}\widetilde{C}^{\Theta E}_{L}\right]\exp(in\varphi_{-\boldsymbol{L},\boldsymbol{\ell}}\pm2i\varphi_{-\boldsymbol{L},\boldsymbol{L}'})$
ΘB	$\left[\mathcal{B}^{(B\Theta)}_{L,(n,p)}\widetilde{C}^{\Theta\Theta}_{L}+\mathcal{B}^{(BE)}_{L,(n,p)}\widetilde{C}^{\Theta E}_{L}\right]\exp(in\varphi_{-\boldsymbol{L},\boldsymbol{\ell}}\pm2i\varphi_{-\boldsymbol{L},\boldsymbol{L}'})$
EE	$\left[\mathcal{B}^{(E\Theta)}_{L,(n,p)}\widetilde{C}^{\Theta E}_{L}+\mathcal{B}^{(EE)}_{L,(n,p)}\widetilde{C}^{EE}_{L}\right]\exp(in\varphi_{-\boldsymbol{L},\boldsymbol{\ell}}\pm2i\varphi_{-\boldsymbol{L},\boldsymbol{L}'})+(\boldsymbol{L}\leftrightarrow\boldsymbol{L}')$
EB	$\left[\mathcal{B}^{(B\Theta)}_{L,(n,p)}\widetilde{C}^{\Theta E}_{L}+\mathcal{B}^{(BE)}_{L,(n,p)}\widetilde{C}^{EE}_{L}\right]\exp(in\varphi_{-\boldsymbol{L},\boldsymbol{\ell}}\pm2i\varphi_{-\boldsymbol{L},\boldsymbol{L}'})+\mathcal{B}^{(EB)}_{L',(n,p)}\widetilde{C}^{BB}_{L'}\exp(in\varphi_{-\boldsymbol{L}',\boldsymbol{\ell}}\pm2i\varphi_{-\boldsymbol{L}',\boldsymbol{L}})$
BB	$\mathcal{B}^{(BB)}_{L,(n,p)}\widetilde{C}^{BB}_{L}\exp(in\varphi_{-\boldsymbol{L},\boldsymbol{\ell}}\pm2i\varphi_{-\boldsymbol{L},\boldsymbol{L}'})+(\boldsymbol{L}\leftrightarrow\boldsymbol{L}')$

first term of equation (36) becomes $b^{+}_{\ell,0}X_{\boldsymbol{\ell}}$. Assuming that $b^{+}_{\ell,0}=1$, the convolution in equation (36) leads to an off-diagonal covariance given by

$$\langle\widehat{X}_{\boldsymbol{L}}\widehat{Y}_{\boldsymbol{L}'}\rangle=\sum_{n\neq0}\sum_{p=0,\pm1}f^{\psi^{(n,p)},(XY)}_{\boldsymbol{\ell},\boldsymbol{L}}\left(\psi^{(n,p)}_{\boldsymbol{\ell}}\right)_{\rm ani}+\mathcal{O}\left[(\psi^{(n,p)})^{2}_{\rm ani}\right], \tag{37}$$

where the weight functions are summarized in Table 3. For $b^{+}_{\ell,0}\neq1$, we can utilize $f^{\psi^{(n,p)},(XY)}_{\boldsymbol{\ell},\boldsymbol{L}}/(b^{+}_{L,0}b^{+}_{L',0})$ for the weight function. Note that the above derivations cover simpler cases. If the beams of two detectors are the same, $b^{-}=0$, with Gaussian shape, $b_{L,\,n}\propto\delta_{n,\,0}$, and if $\widehat{\alpha}_{t}$ is the same for all measurements, we obtain $\widehat{\Xi}^{(\pm2)}(\hat{\boldsymbol{n}})=\Xi^{(\pm2)}(\hat{\boldsymbol{n}})\mathrm{e}^{\pm2\mathrm{i}\delta(\hat{\boldsymbol{n}})}$. We also note that, for the temperature-only case, the results are consistent with our previous work.

3.2 Mean-field biases

All of the above contaminations lead to the mean-field bias for lensing estimator, $\widehat{x}^{(XY)}_{\boldsymbol{\ell}}$. Omitting the subscript (XY), the mean-field biases are given by

$$\begin{aligned}\langle\widehat{x}_{\boldsymbol{\ell}}\rangle&=A^{xx}_{\ell}\int\frac{\mathrm{d}^{2}\boldsymbol{L}}{(2\pi)^{2}}\,g^{x}_{\boldsymbol{\ell},\boldsymbol{L}}\langle\overline{X}_{\boldsymbol{L}}\overline{Y}_{\boldsymbol{L}'}\rangle\\&=A^{xx}_{\ell}\int\frac{\mathrm{d}^{2}\boldsymbol{L}}{(2\pi)^{2}}\sum_{y}g^{x}_{\boldsymbol{\ell},\boldsymbol{L}}f^{y}_{\boldsymbol{\ell},\boldsymbol{L}}y_{\boldsymbol{\ell}}\\&=\sum_{y}R^{xy}_{\ell}y_{\boldsymbol{\ell}},\end{aligned} \tag{38}$$

where $y=M$, S or $\psi^{(n,p)}$. Also, we define the response function R_{ℓ} and normalization A_{ℓ} as

$$R^{xy}_{\ell}=\frac{A^{xx}_{\ell}}{A^{xy}_{\ell}};\qquad A^{xy}_{\ell}=\left[\int\frac{\mathrm{d}^{2}\boldsymbol{L}}{(2\pi)^{2}}\,g^{x}_{\boldsymbol{\ell},\boldsymbol{L}}f^{y}_{\boldsymbol{\ell},\boldsymbol{L}'}\right]^{-1}. \tag{39}$$

3.3 Bias-hardened estimator

Estimators that are bias-hardened against the above effects can be constructed analogously to the temperature case. That is, we first construct a naïve estimator for a given effect y as

$$\widehat{y}_{\boldsymbol{\ell}}=A^{yy}_{\ell}\int\frac{\mathrm{d}^{2}\boldsymbol{L}}{(2\pi)^{2}}\,g^{y}_{\boldsymbol{\ell},\boldsymbol{L}}\overline{X}_{\boldsymbol{L}}\overline{Y}_{\boldsymbol{L}'}, \tag{40}$$

where $g^{y}_{\boldsymbol{\ell},\boldsymbol{L}}$ and A^{yy}_{ℓ} are defined as equations (9) and (10), respectively, but using the weight function, $f^{y,(XY)}_{\boldsymbol{\ell},\boldsymbol{L}}$, instead of the lensing weight function, $f^{x,(XY)}_{\boldsymbol{\ell},\boldsymbol{L}}(x=\phi,\varpi)$. This estimator for y_{ℓ} is in turn biased by lensing. We can then obtain a bias-hardened estimator as

$$\widehat{x}^{\rm (BHE)}_{\boldsymbol{\ell}}\equiv\sum_{y}\left\{\mathbf{R}^{-1}_{\ell}\right\}^{x,y}\widehat{y}_{\boldsymbol{\ell}}. \tag{41}$$

4 DEMONSTRATION OF BIAS-HARDENED ESTIMATOR FOR MEAN-FIELD BIAS

In this section, we discuss whether the bias-hardened estimator for lensing fields can be used as a cross-check for the conventional estimator. For this purpose, first we compute the case where the mean field is generated only from the effect of masking. One concern here is the validity of linear-order approximation. That is, to derive the bias-hardened estimator, we have ignored any higher-order terms of M_{L} (and, of course, for other non-lensing fields).

4.1 Simulated maps and analysis

We use simulated polarization maps produced using methods similar to our previous work (Namikawa et al. 2013a). For lensing reconstruction, we use 100 realizations of lensed Stokes Q and U maps, simulated on a 5×5 deg^{2} patch. The details of the method used to generate these lensed maps are described in Appendix B. To simulate the masking of point sources, we create masks by cutting 200 regions of randomly located 10×10 arcmin^{2} squares. Note that the area covered by the point-source masks is ∼5 per cent of

total area, and the percentage roughly corresponds to that used in the South Pole Telescope (SPT) polarization analysis (Hanson et al. 2013). To consider experiments with high-angular resolution such as SPTpol, PolarBear and ACTPol, as well as to avoid contamination by the Sunyaev–Zel'dovich effect (Zel'dovich & Sunyaev 1969) and unresolved point sources, we assume a delta function instrumental beam. The E- and B-mode multipoles are used at $2 \leq \ell \leq 3000$. We assume homogeneous map noise, with a level of 0.01 μK arcmin. Note that, even in the presence of inhomogeneous noise, by combining the bias-hardened estimator described in Section 3.1.2, the mean field due to inhomogeneous noise would be reduced as already applied to the lensing reconstruction with the Planck temperature map [Ade et al. (Planck Collaboration) 2013b], and the qualitative result would be similar to that obtained in this paper.

4.2 Filtering

For the conventional estimator approach, we experiment with the following filtering techniques to suppress the mask-mean field: apodization of the survey boundary and C^{-1} filtering for the point-source holes.

4.2.1 *Apodization window function*

In our analysis, we use the following analytical apodization function, whose value and derivatives are zero at the boundaries of the survey region:

$$W(x, y; s_0) = w(x; s_0) w(y; s_0) M(x, y). \tag{42}$$

Here, $w(s; s_0)$ is a sine apodization function given by

$$w(s; s_0) = \begin{cases} 1 & |s| < a s_0 \\ \frac{1-|s|/a}{1-s_0} - \frac{1}{2\pi} \sin\left(2\pi \frac{1-|s|/a}{1-s_0}\right) & a s_0 \leq |s| < a \\ 0 & a \leq |s| \end{cases}, \tag{43}$$

and $M(x, y)$ represents the point-source mask [i.e. 0 at the presence of (resolved) point sources, and otherwise 1]. The parameter, s_0, indicates the width of the region where the apodization is applied.

4.2.2 C^{-1} *filtering*

The minimum-variance filtering that emerges from likelihood-based derivations of lensing estimators is known as C^{-1} filtering. The inverse-variance filtered Fourier modes, $\bar{\boldsymbol{X}}_\ell = (E_\ell, B_\ell)$, are obtained by solving

$$\left(1 + \mathbf{C}^{1/2} \mathbf{N}^{-1} \mathbf{C}^{1/2}\right) (\mathbf{C}^{1/2} \bar{\boldsymbol{X}}) = \mathbf{C}^{1/2} \mathbf{N}^{-1} \hat{X}, \tag{44}$$

where $\bar{\boldsymbol{X}}$ is a vector whose components are $\bar{X}_\ell$, $\mathbf{C}$ is the covariance of the CMB anisotropies with

$$\{\boldsymbol{C}\}_{\ell_i, \ell_j} = \delta_{\ell_i - \ell_j} \begin{pmatrix} C_{\ell_i}^{EE} & 0 \\ 0 & C_{\ell_i}^{BB} \end{pmatrix}, \tag{45}$$

and $\boldsymbol{N} = \langle \boldsymbol{n}^\dagger \boldsymbol{n} \rangle$ is the covariance matrix for the instrumental noise. The noise covariance matrix in Fourier space is obtained from that in real space as

$$\boldsymbol{N}^{-1} = \boldsymbol{Y}^\dagger \overline{\boldsymbol{N}}^{-1} \boldsymbol{Y}, \tag{46}$$

where the pointing matrix, $\boldsymbol{Y}$, is defined by

$$\{\boldsymbol{Y}\}_{\hat{\boldsymbol{n}}_i, \boldsymbol{\ell}_j} = \exp(\mathrm{i} \hat{\boldsymbol{n}}_i \cdot \boldsymbol{\ell}_j) \exp(-2\varphi_{\ell_j}) \begin{pmatrix} 1 & \mathrm{i} \\ 1 & -\mathrm{i} \end{pmatrix}. \tag{47}$$

Note that the matrix in equation (47) describes the transformation of $(E_\ell, B_\ell)^t$ to $(E_\ell + \mathrm{i} B_\ell, E_\ell - \mathrm{i} B_\ell)^t$. The mask is incorporated by setting the noise level of masked pixels to infinity, and therefore the inverse of the noise covariance in real space $\overline{\boldsymbol{N}}^{-1}$ to zero for masked pixels. The inversion of the matrix on the left-hand side of equation (44) can be numerically costly, but can be evaluated using conjugate descent with careful preconditioning (Smith et al. 2007). Because the mask mean field due to the survey boundary remains after applying the C^{-1} filter, we additionally apply an apodizing function given by equation (43).

4.3 Mean-field bias due to masking

We now discuss the mean-field bias generated by masking.

Given N realizations of estimator, $\widehat{x}_\ell^{i,(XY)}$ $(i = 1, 2, \ldots, N)$, we define the mean-field power spectrum as

$$\mathcal{M}_\ell^{x,(XY)} = \frac{1}{W_4} \int \frac{\mathrm{d}\varphi_\ell}{2\pi} \left| \frac{1}{N} \sum_{i=1}^{N} \widehat{x}_\ell^{i,(XY)} \right|^2, \tag{48}$$

where the quantity W_4 is the normalization correction for effect of window function as

$$W_4 = \int \mathrm{d}^2 \hat{\boldsymbol{n}} \, [W(\hat{\boldsymbol{n}})]^4. \tag{49}$$

With N-realizations of CMB maps, the mean field becomes (Benoit-Levy et al. 2013)

$$\mathcal{M}_\ell^{x,(XY)} \simeq \frac{1}{W_4} \int \frac{\mathrm{d}\varphi_\ell}{2\pi} |\langle \widehat{x}_\ell^{(XY)} \rangle|^2 + \frac{A_\ell^{xx,(XY)} + C_\ell^{xx}}{N}. \tag{50}$$

The resulting mask mean fields for $\widehat{\phi}$ are shown in Figs 1 and 2 for the quadratic combinations of EE and EB cases, respectively. We compare results between the case with and without the bias-hardened estimator for the mitigating mask mean field. We also vary the apodization parameter, s_0, introduced in equation (43). The Monte Carlo noise floor is the second term of equation (50). For EE, the mask mean field is large on large angular scales, and exceeds the expected lensing power. We can clearly see that the bias-hardened estimator works well to mitigate the mask mean field. However, the EB estimator has small contributions to the mask mean field. The reason for this is as follows. If we use the filtering methods, the quantity M_ℓ has a value of only around $\ell \sim 0$, and thus the mask mean field, which is expressed as $R_\ell^{xM} M_\ell$, is significant only for $\ell \sim 0$. For the EB estimator, however, the response function, R_ℓ^{xM}, given in equation (39), has the sine function involved in the weight function, $f_{\ell,L}^{x,(EB)}$, and goes to zero as $\ell \to 0$. This is contrary to the case of the EE estimator in which the weight function includes the cosine function instead of the sine function. Note that the origin of the sine function in the weight function is the parity of EB cross-correlation (i.e. odd parity symmetry), because the weight function is given by equation (7). We have also checked that, because the behaviour of the response function for ΘB is similar to that of EB, the mask mean field is negligible for the ΘB estimator. As expected, the mask mean field on the curl mode shown in Fig. 3 would also be negligible for both EE and EB estimators.

The residual mean-field bias also affects the power spectrum estimation through

$$\int \frac{\mathrm{d}\varphi_\ell}{2\pi} |\widehat{x}_\ell|^2 = \mathcal{M}_\ell^x + A_\ell^{xx} + C_\ell^{xx}. \tag{51}$$

The figure shows that, for EE, the conventional estimator generates a significant mask mean field, which exceeds the lensing power

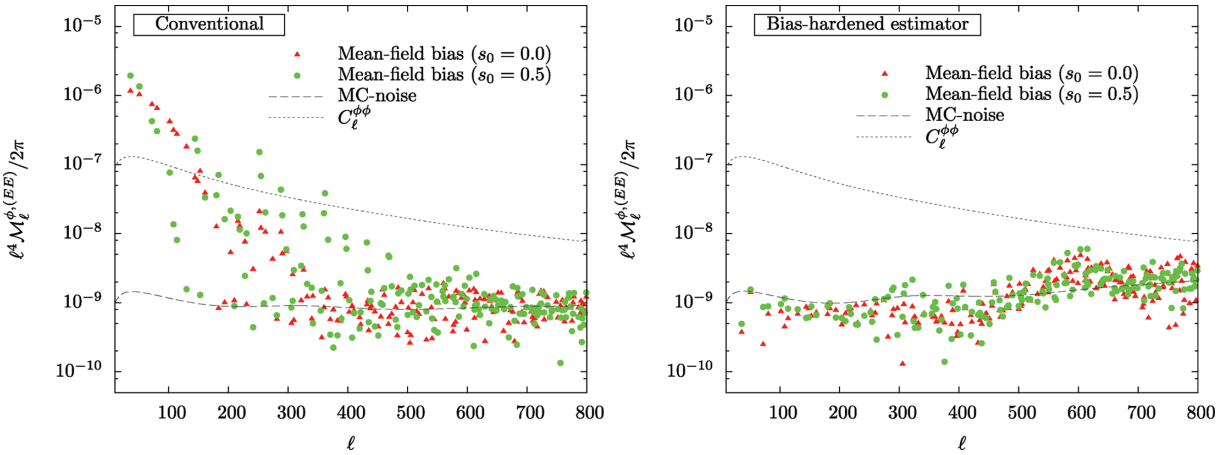

Figure 1. Mean-field power spectrum for the gradient-mode *EE* estimator, $\mathcal{M}_\ell^{\phi,(EE)}$, estimated with 100 lensed simulated maps. The left panel shows results with the conventional estimator, varying the apodization parameter, s_0, as 0.0 and 0.5. The Monte Carlo noise floors (dashed line) are shown comparing with the mean-field power spectrum. The theoretical lensing power spectrum is also shown as a solid grey line. Note that the reconstruction is performed on $(5\,\mathrm{deg})^2$, with *E*-mode multipoles ranges of $2 \leq \ell \leq 3000$. The right panel is the same as the left panel but with the bias-hardened estimator.

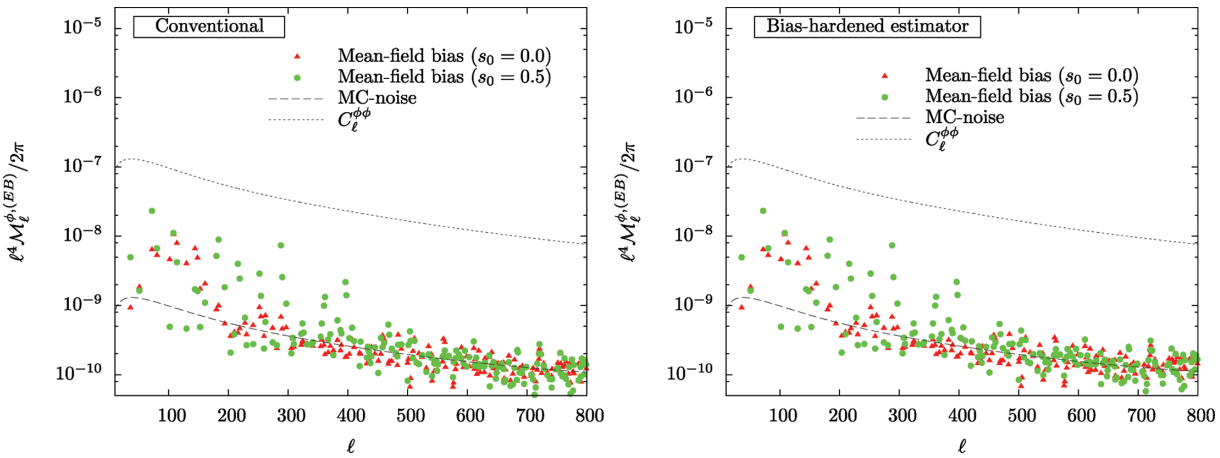

Figure 2. Same as Fig. 1, but for the *EB* case.

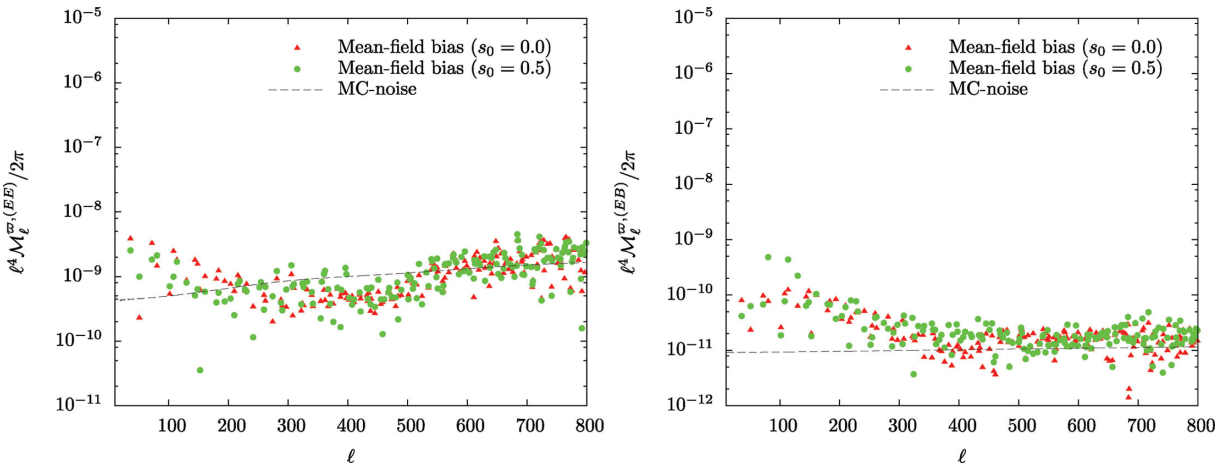

Figure 3. Mean-field power spectrum for curl modes with *EE* (left) and *EB* (right) estimators. The Monte Carlo noise floors are shown with dashed lines.

spectrum; the lensing power spectrum estimation could therefore suffer from uncertainties in the mean-field correction. However, the bias-hardened estimator significantly suppresses the mask mean field, which is below the lensing power spectrum.

4.4 Mean-field bias due to polarization angle

The mask mean field for the *EB* estimator is negligible even for the case with a simple apodization function. However, the mean-field

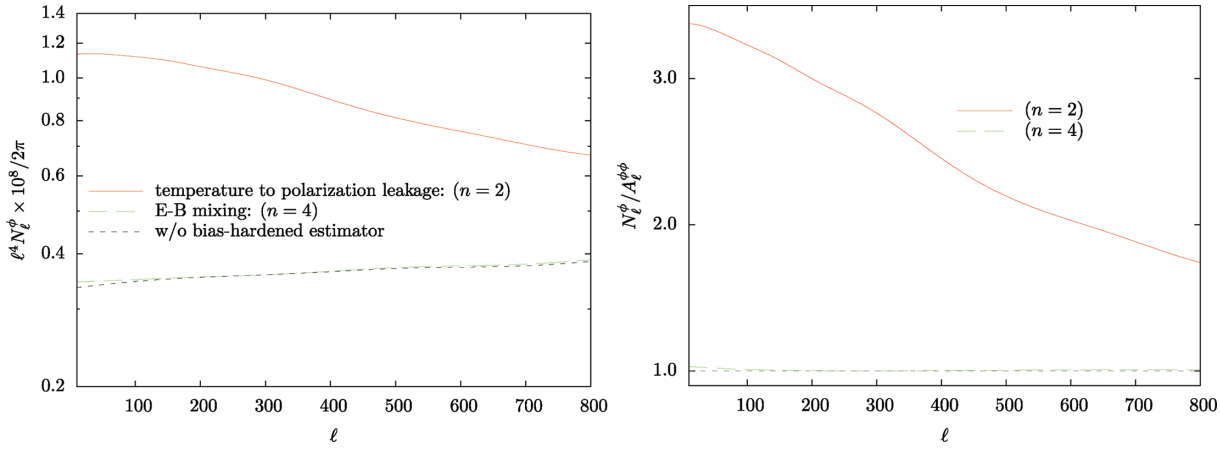

Figure 4. Left: comparison of the noise level of lensing reconstruction between the case with and without the bias-hardened estimator for *EB* case. The noise level of the bias-hardened estimator, N_ℓ^ϕ, is computed from equation (57). The labels, $n = 2$ and $n = 4$, denote the temperature to polarization leakage, and $E - B$ mixing by the rotation of the coordinate system, respectively (see the text for the definitions and details). Right: the ratio of the noise level described in the left panel compared to the case without the bias-hardened estimator, $N_\ell^\phi / A_\ell^{\phi\phi}$.

biases can be generated from other sources, such as polarization angle errors. Here, to see the potential of bias-hardened estimators to mitigate polarization angle systematics, we compute a rough estimation of the response function and degradation of noise level for the *EB* estimator.

For a two-beam experiment, with $b^- \neq 0$ and $b_{L,n} \propto \delta_{n,0}$, as an example, we consider the following non-zero weight functions for the *EB* estimator:

$$f_{\ell,L}^{\psi^{(\pm2,\mp1)}} = \mp \mathrm{i}\, \mathrm{e}^{\pm 2\mathrm{i}\varphi_{L',\ell}} b_{L,0}^- \widetilde{C}_L^{\Theta E} \tag{52}$$

$$f_{\ell,L}^{\psi^{(\pm4,\mp1)}} = \pm \mathrm{i}\, \mathrm{e}^{\pm 2\mathrm{i}(\varphi_{L,\ell}+\varphi_{L',\ell})} \left(b_{L,0} \widetilde{C}_L^{BB} + b_{L',0} \widetilde{C}_{L'}^{EE} \right), \tag{53}$$

where we have omitted the label, (*EB*), in the weight functions. Note that the cases with $(n, p) = (\pm2, \mp1)$ and $(\pm4, \mp1)$ denote the systematics due to temperature to polarization leakage and $E - B$ mode mixing, respectively. In general, as an alternative to $\psi_\ell^{(n,p)}$, we can use the following quantities:

$$\psi_\ell^{(n,\varepsilon)} = \psi_\ell^{(-n,+1)} + (-1)^n \psi_\ell^{(n,-1)}, \tag{54}$$

$$\psi_\ell^{(n,\beta)} = -\mathrm{i} \left[\psi_\ell^{(-n,+1)} - (-1)^n \psi_\ell^{(n,-1)} \right], \tag{55}$$

where the above quantities satisfy $(\psi_\ell^{(n,\varepsilon)})^* = \psi_{-\ell}^{(n,\varepsilon)}$ and $(\psi_\ell^{(n,\beta)})^* = \psi_{-\ell}^{(n,\beta)}$. The corresponding weight functions for $\psi_\ell^{(n,\varepsilon)}$ and $\psi_\ell^{(n,\beta)}$ are

$$\begin{aligned}
f_{\ell,L}^{\psi^{(2,\varepsilon)}} &= b_{L,0}^- \sin(2\varphi_{L',\ell}) \widetilde{C}_L^{\Theta E}, \\
f_{\ell,L}^{\psi^{(2,\beta)}} &= -b_{L,0}^- \cos(2\varphi_{L',\ell}) \widetilde{C}_L^{\Theta E}, \\
f_{\ell,L}^{\psi^{(4,\varepsilon)}} &= -\sin(2\varphi_{L,\ell} + 2\varphi_{L',\ell}) \left(b_{L,0} \widetilde{C}_L^{BB} + b_{L',0} \widetilde{C}_{L'}^{EE} \right), \\
f_{\ell,L}^{\psi^{(4,\beta)}} &= \cos(2\varphi_{L,\ell} + 2\varphi_{L',\ell}) \left(b_{L,0} \widetilde{C}_L^{BB} + b_{L',0} \widetilde{C}_{L'}^{EE} \right).
\end{aligned} \tag{56}$$

In our calculation, for simplicity, we assume $b_{L,0}^- \equiv \epsilon b_{L,0}$ and a top-hat function for $b_{L,0}$ (i.e. $b_{L,0} = 1$ for $\ell \leq 3000$, and 0 otherwise). We also ignore $\widetilde{C}_L^{BB}$ in the above equation. Because the weight functions of $\psi_\ell^{(n,\beta)}$ are obtained only by replacing the sine function in $f_{\ell,L}^{(n,\varepsilon)}$ with the cosine function, we expect that the amplitude of the noise level for $\psi_\ell^{(n,\beta)}$ would not be so different from that for $\psi_\ell^{(n,\varepsilon)}$. Thus, we only focus on the case to mitigate $\psi_\ell^{(n,\varepsilon)}$ in the following calculations.

In the left panel of Fig. 4, we show the noise level for the bias-hardened estimator incorporating polarization angle systematics of $\psi_\ell^{(n,\varepsilon)}$. The noise level for the conventional approach corresponds to the normalization, $A_\ell^{\phi\phi}$. However, with $n = 2$ and 4, the noise level for the bias-hardened estimator is given by

$$N_\ell^\phi = \frac{A_\ell^{\phi\phi}}{1 - R_\ell^{\phi\psi^{(n,\varepsilon)}} R_\ell^{\psi^{(n,\varepsilon)}\phi}}, \tag{57}$$

where the response functions, $R^{\phi\psi^{(n,\varepsilon)}}$ and $R^{\psi^{(n,\varepsilon)}\phi}$, defined in equation (39), are computed with the weight functions given in equation (56). Note that the noise level does not depend on ϵ. We find that the noise level is not necessarily much larger using a bias-hardened estimator compared to the conventional approach. In the right panel, we also show the ratio of the case with the bias-hardened estimator to that with conventional estimator. We find that the degradation of noise level is only up to $\lesssim$1 per cent for $n = 4$, and by a factor of $\sim$3 for $n = 2$. Our results imply that the bias-hardened estimator is enough to utilize for a cross-check of the usual method for polarization angle systematics.

5 SUMMARY

We have discussed methods for mitigating the mean-field bias in the case of lensing reconstruction with CMB polarization. First, we derived the mean-field bias generated from masking, inhomogeneous noise (and/or unresolved point sources) and polarization angle systematics associated with the asymmetric beam shape, in analogy to the temperature-only case. Then, we performed numerical tests to see how significantly the mean-field bias from masking is mitigated with the bias-hardened estimator. We found that, for the *EE* estimator, it is particularly useful for the reduction of the large-scale component of the mean field. However, for the *EB* estimator, we found that the amplitude of the mask mean field is negligible compared to the lensing signal. The bias-hardened *EB* estimator is useful for other potential sources of mean field, such as polarization angle systematics, and we have shown that the increase of the noise level is only up to 1 per cent for $n = 4$ ($E - B$ mixing), and by a factor of $\sim$3 for $n = 2$ (temperature to polarization leakage), compared to the conventional approach.

ACKNOWLEDGEMENTS

We are very grateful to Duncan Hanson for valuable comments and helpful discussions. We are also grateful to Takashi Hamana and Takahiro Nishimichi for kindly providing the ray-tracing simulation code and the 2LPT code, and we thank Ryo Nagata for useful comments. This work was supported in part by Grant-in-Aid for Scientific Research on Priority Areas No. 467 'Probing the Dark Energy through an Extremely Wide and Deep Survey with Subaru Telescope', by the MEXT Grant-in-Aid for Scientific Research on Innovative Areas (No. 22111501), by the Japan Society for the Promotion of Science (JSPS) Grant-in-Aid for Research Activity Start-up (No. 80708511), and by JSPS Grant-in-Aid for Scientific Research (B) (No. 25287062) 'Probing the Origin of Primordial Mini-haloes via Gravitational Lensing Phenomena'. Numerical computations were carried out on the SR16000 at the Yukawa Institute for Theoretical Physics (YITP), Kyoto University and on the Cray XT4 at the Center for Computational Astrophysics (CfCA), National Astronomical Observatory of Japan.

REFERENCES

Abazajian K. et al., 2013, preprint (arXiv:1309.5383)
Ade P. et al. (Planck Collaboration), 2013a, preprint (arXiv:1303.5076)
Ade P. et al. (Planck Collaboration), 2013b, preprint (arXiv:1303.5077)
Ade P. et al. (Planck Collaboration), 2013c, preprint (arXiv:1303.5078)
Amendola L., 1996, MNRAS, 283, 983
Anderes E., 2013, Phys. Rev. D, 88, 083517
Battye R. A., Moss A., 2013, preprint (arXiv:1308.5870)
Benoit-Levy A., Dechelette T., Benabed K., Cardoso J.-F., Hanson D., Prunet S., 2013, A&A, 555, 10
Bleem L. et al., 2012, ApJ, 753, L9
Carvalho C. S., Tereno I., 2011, Phys. Rev. D, 84, 063001
Cooray A., Kamionkowski M., Caldwell R. R., 2005, Phys. Rev. D, 71, 123527
Das S. et al., 2011, Phys. Rev. Lett., 107, 021301
Das S. et al., 2013, preprint (arXiv:1301.1037)
Geach J. et al., 2013, ApJ, 776, L41
Hamana T., Mellier Y., 2001, MNRAS, 327, 169
Hanson D., Rocha G., Gorski K., 2009, MNRAS, 400, 2169
Hanson D., Lewis A., Challinor A., 2010, Phys. Rev. D, 81, 103003
Hanson D., Challinor A., Efstathiou G., Bielewicz P., 2011, Phys. Rev. D, 83, 043005
Hanson D. et al., 2013, Phys. Rev. Lett., 111, 141301
Hirata C. M., Seljak U., 2003, Phys. Rev. D, 68, 083002
Hirata C. M., Ho S., Padmanabhan N., Seljak U., Bahcall N. A., 2008, Phys. Rev. D, 78, 043520
Holder G. et al., 2013, ApJ, 771, L16
Hu W., 2001, Phys. Rev. D, 64, 083005
Hu W., Okamoto T., 2002, ApJ, 574, 566
Jeong D., Komatsu E., Jain B., 2009, Phys. Rev. D, 80, 123527
Joudaki S., Kaplinghat M., 2012, Phys. Rev. D, 86, 023526
Kesden M., Cooray A., Kamionkowski M., 2002, Phys. Rev. Lett., 89, 011304
Knox L., Song Y.-S., 2002, Phys. Rev. Lett., 89, 011303
Lewis A., Challinor A., 2006, Phys. Rep., 429, 1
Lewis A., Challinor A., Lasenby A., 2000, ApJ, 538, 473
Lewis A., Challinor A., Hanson D., 2011, J. Cosmol. Astropart. Phys., 1103, 018
Namikawa T., Saito S., Taruya A., 2010, J. Cosmol. Astropart. Phys., 1012, 027
Namikawa T., Yamauchi D., Taruya A., 2012, J. Cosmol. Astropart. Phys., 1201, 007
Namikawa T., Hanson D., Takahashi R., 2013a, MNRAS, 431, 609
Namikawa T., Yamauchi D., Taruya A., 2013b, Phys. Rev. D, 88, 083525
Okamoto T., Hu W., 2003, Phys. Rev. D, 67, 083002
Perotto L., Bobin J., Plaszczynski S., Starck J.-L., Lavabre A., 2010, A&A, 519, A4
Plaszczynski S., Lavabre A., Perotto L., Starck J.-L., 2012, A&A, 544, A27
Regan D., Shellard E., Fergusson J., 2010, Phys. Rev. D, 82, 023520
Seljak U., Zaldarriaga M., 1999, Phys. Rev. Lett., 82, 2636
Sherwin B. D., Das S., 2010, preprint (arXiv:1011.4510)
Sherwin B. D. et al., 2011, Phys. Rev. Lett., 107, 021302
Sherwin B. D. et al., 2012, Phys. Rev. D, 86, 083006
Shimon M., Keating B., Ponthieu N., Hivon E., 2008, Phys. Rev. D, 77, 083003
Smith K. M., 2006, New Astron. Rev., 50, 1025
Smith K. M., Zaldarriaga M., 2007, Phys. Rev. D, 76, 043001
Smith K. M., Zahn O., Dore O., 2007, Phys. Rev. D, 76, 043510
Takeuchi Y., Ichiki K., Matsubara T., 2012, Phys. Rev. D, 85, 043518
van Engelen A. et al., 2012, ApJ, 756, 142
Wilkinson R. J., Lesgourgues J., Boehm C., 2013, preprint (arXiv:1309.7588)
Yamauchi D., Namikawa T., Taruya A., 2012, J. Cosmol. Astropart. Phys., 1210, 030
Yamauchi D., Namikawa T., Taruya A., 2013, J. Cosmol. Astropart. Phys., 1308, 051
Zaldarriaga M., Seljak U., 1999, Phys. Rev. D, 59, 123507
Zel'dovich Y., Sunyaev R., 1969, Ap&SS, 4, 301

APPENDIX A: BIAS-HARDENED ESTIMATOR FOR LENSING POWER SPECTRUM

Here, we present an optimal estimator for the lensing angular power spectrum, $\widehat{C}^{xx}_{\ell}$, motivated by the maximum likelihood estimator for lensing trispectrum, as proposed in our previous work (Namikawa et al. 2013a), where we considered the temperature anisotropies alone.

A1 Formalism

A1.1 Likelihood for lensed CMB anisotropies

The Gaussian probability distribution function for temperature and polarization fields, $a = \Theta$, E or B, whose covariance matrices are $\boldsymbol{C}^{a_\ell, b_{\ell'}} = \langle a_\ell b_{\ell'} \rangle$, is given by

$$P_{\rm g} = \frac{1}{\sqrt{(2\pi)^N \det \boldsymbol{C}}} \exp\left[-\frac{1}{2} \sum_{ab} \sum_{\ell,\ell'} a_\ell (\boldsymbol{C}^{-1})^{a_\ell, b_{\ell'}} b_{\ell'} \right]. \quad \text{(A1)}$$

Because the lensed anisotropies, $\widetilde{\Theta}$, $\widetilde{E}$ and $\widetilde{B}$, are no longer the Gaussian fields, the perturbative expansion of the likelihood for the lensed anisotropies at leading order is given as (Amendola 1996; Regan, Shellard & Fergusson 2010)

$$P = \left(1 + \sum_{abcd} \sum_{\ell_i} \langle a_{\ell_1} b_{\ell_2} c_{\ell_3} d_{\ell_4} \rangle_{\rm c} \frac{\partial}{\partial a_{\ell_1}} \frac{\partial}{\partial b_{\ell_2}} \frac{\partial}{\partial c_{\ell_3}} \frac{\partial}{\partial d_{\ell_4}} \right) P_{\rm g}. \quad \text{(A2)}$$

Here, we ignore the three-point correlation because this is generated due to the correlation between the integrated Sachs–Wolfe effect and lensing. The cumulant is given by

$$\begin{aligned} \langle a_{\ell_1} b_{\ell_2} c_{\ell_3} d_{\ell_4} \rangle_{\rm c} \simeq\ & f^{ab}_{\ell_{12},\ell_1} f^{cd}_{-\ell_{12},\ell_3} C^{\phi\phi}_{|\ell_{12}|} \delta_{\ell_{12},-\ell_{34}} \\ & + f^{ac}_{\ell_{13},\ell_1} f^{bd}_{-\ell_{13},\ell_2} C^{\phi\phi}_{|\ell_{13}|} \delta_{\ell_{13},-\ell_{24}} \\ & + f^{ad}_{\ell_{14},\ell_1} f^{bc}_{-\ell_{14},\ell_2} C^{\phi\phi}_{|\ell_{14}|} \delta_{\ell_{14},-\ell_{23}}. \end{aligned} \quad \text{(A3)}$$

Substituting equation (A3) into equation (A2), we obtain the probability distribution function for lensed CMB anisotropies. Note here

that we do not compute higher-order terms of $C_\ell^{\phi\phi}$, because we use an approximation that requires an expression only up to the first order of $C_\ell^{\phi\phi}$.

A1.2 Derivative of probability distribution function

To obtain the maximum likelihood point, we differentiate P with respect to C_ℓ^{xx}, and obtain

$$\frac{\partial P}{\partial C_\ell^{xx}} = \sum_{abcd}\left(\widehat{f}_\ell^{ab}\widehat{f}_{-\ell}^{cd} + \widehat{f}_\ell^{ac}\widehat{f}_{-\ell}^{bd} + \widehat{f}_\ell^{ad}\widehat{f}_{-\ell}^{bc}\right)P_{\rm g}, \tag{A4}$$

where the operator is defined as

$$\widehat{f}_\ell^{ab} \equiv \sum_{\ell_1} f_{\ell,\ell_1}^{ab}\frac{\partial}{\partial a_{\ell_1}}\frac{\partial}{\partial b_{\ell-\ell_1}}. \tag{A5}$$

We find that

$$\widehat{f}_\ell^{ab}P_{\rm g} = \left(\overline{x}_\ell^{ab} - \langle\overline{x}_\ell^{ab}\rangle\right)P_{\rm g}, \tag{A6}$$

where we define the unnormalized estimator as

$$\overline{x}_\ell^{ab} = \sum_{\ell_1} f_{\ell,\ell_1}^{ab}\overline{a}_{\ell_1}\overline{b}_{\ell-\ell_1}, \tag{A7}$$

with the inverse variance filtered multipoles as $\overline{a}_\ell = \sum_{a',\ell'}(\mathbf{C}^{-1})^{a\ell a'\ell'}a'_{\ell'}$. Operating $\widehat{f}_{-\ell}^{cd}$ again to equation (A6), we obtain

$$\frac{1}{P_{\rm g}}\widehat{f}_{-\ell}^{cd}\widehat{f}_\ell^{ab}P_{\rm g} = \overline{x}_\ell^{ab,(C)}\overline{x}_{-\ell}^{cd,(C)} - n_\ell^{ab,cd}, \tag{A8}$$

where the mean-field corrected estimator and its reconstruction noise bias are given by

$$\overline{x}_\ell^{ab,(C)} \equiv \overline{x}_\ell^{ab} - \langle\overline{x}_\ell^{ab}\rangle \tag{A9}$$

$$n_\ell^{ab,cd} \equiv \left\langle\left[\overline{x}_\ell^{a^{(1)}b} + \overline{x}_\ell^{ab^{(1)}}\right]\left[\overline{x}_{-\ell}^{c^{(1)}d} + \overline{x}_{-\ell}^{cd^{(1)}}\right]\right\rangle_{(1)} - \frac{1}{2}\left\langle\left[\overline{x}_\ell^{a^{(1)}b^{(2)}} + \overline{x}_\ell^{a^{(2)}b^{(1)}}\right]\left[\overline{x}_{-\ell}^{c^{(1)}d^{(2)}} + \overline{x}_{-\ell}^{c^{(2)}d^{(1)}}\right]\right\rangle_{(1),(2)}, \tag{A10}$$

where index (i) denotes the simulated maps obtained from ith set of the Monte Carlo simulation, and $\langle\cdots\rangle_{(i)}$ denotes the ensemble average for the ith set of the Monte Carlo simulation. Note here that $\langle n_\ell^{ab,cd}\rangle$ corresponds to the disconnected part of $\langle\overline{x}_\ell^{ab,(C)}\overline{x}_{-\ell}^{cd,(C)}\rangle$. We then obtain the derivative of a log-likelihood, $\mathcal{L} = \ln P$, as

$$\frac{\partial\mathcal{L}}{\partial C_\ell^{xx}} = \frac{1}{P}\frac{\partial P}{\partial C_\ell^{xx}} \simeq \frac{1}{P_{\rm g}}\frac{\partial P}{\partial C_\ell^{xx}} = \sum_{abcd}\left[\overline{x}_\ell^{ab,(C)}\overline{x}_{-\ell}^{cd,(C)} - n_\ell^{ab,cd} + (a\leftrightarrow c) + (a\leftrightarrow d)\right]. \tag{A11}$$

A1.3 Temperature

Here, we consider the case of temperature alone (or $a = b = c = d \equiv X$). With equation (A11), the derivative of a log-likelihood, $\mathcal{L} = \ln P$, is

$$\frac{\partial\mathcal{L}}{\partial C_\ell^{xx}} = 3\left[|\overline{x}_\ell^{(C)}|^2 - n_\ell\right], \tag{A12}$$

where we drop the index, X, in the unnormalized estimator and disconnected bias. Equation (A12) motivates an unbiased estimator

$$\widehat{C}_\ell^{xx} = \left(\frac{A_\ell}{2}\right)^2\left[|\overline{x}_\ell^{(C)}|^2 - n_\ell\right] = |\widehat{x}_\ell^{(C)}|^2 - \widehat{n}_\ell, \tag{A13}$$

where

$$\widehat{x}_\ell^{(C)} = \frac{A_\ell}{2}\sum_{\ell_1} f_{\ell,\ell_1}\overline{\Theta}_{\ell_1}\overline{\Theta}_{\ell-\ell_1} \tag{A14}$$

$$\widehat{n}_\ell = 2\left[2\left\langle\widehat{x}_\ell^{\Theta^{(1)}\Theta}\widehat{x}_{-\ell}^{\Theta^{(1)}\Theta}\right\rangle_{(1)} - \left\langle\widehat{x}_\ell^{\Theta^{(1)}\Theta^{(2)}}\widehat{x}_{-\ell}^{\Theta^{(1)}\Theta^{(2)}}\right\rangle_{(1),(2)}\right]. \tag{A15}$$

The above equation coincides with Namikawa et al. (2013a), and is generalized for the cases using only lensed *E*/*B* modes alone.

A1.4 Temperature and polarizations

We now generalize the case including polarizations. Equation (A11) implies that, for each combination of (a, b) and (c, d), we can construct the lensing power spectrum estimator as

$$\widehat{C}_\ell^{ab,cd} = \widehat{x}_\ell^{ab,(C)}\widehat{x}_{-\ell}^{cd,(C)} - \widehat{n}_\ell^{ab,cd}, \tag{A16}$$

where the first term is the power spectrum of the usual quadratic estimator but the second term is the estimator for the disconnected bias, $\widehat{n}^{ab,cd}$, defined as

$$\widehat{n}_\ell^{ab,cd} = \left\langle\left[\widehat{x}_\ell^{a^{(1)}b} + \widehat{x}_\ell^{ab^{(1)}}\right]\left[\widehat{x}_{-\ell}^{c^{(1)}d} + \widehat{x}_{-\ell}^{cd^{(1)}}\right]\right\rangle_{(1)} - \frac{1}{2}\left\langle\left[\widehat{x}_\ell^{a^{(1)}b^{(2)}} + \widehat{x}_\ell^{a^{(2)}b^{(1)}}\right]\left[\widehat{x}_{-\ell}^{c^{(1)}d^{(2)}} + \widehat{x}_{-\ell}^{c^{(2)}d^{(1)}}\right]\right\rangle_{(1),(2)}. \tag{A17}$$

Denoting $\alpha, \beta = abcd$, an optimal estimator would be obtained by combining all combinations of $abcd$ as

$$\widehat{C}_\ell^{xx} = N_\ell^{xx}\sum_{\alpha,\beta}\left\{(N_\ell^{xx})^{-1}\right\}^{\alpha,\beta}\widehat{C}_\ell^{\alpha}, \tag{A18}$$

where the optimal noise level and noise covariance matrix are given by

$$N_\ell^{xx} \equiv \sum_{\beta,\beta'}\{(\mathbf{N}_\ell^{xx})^{-1}\}_{\beta,\beta'}; \qquad \{\mathbf{N}_\ell\}^{\alpha,\beta} = \left\langle\widehat{C}_\ell^{\alpha}\widehat{C}_\ell^{\beta}\right\rangle. \tag{A19}$$

APPENDIX B: NUMERICAL SIMULATION OF LENSED CMB MAPS

In this section, we briefly present our procedure to prepare lensed CMB maps. Our procedure is the same as for the lensed CMB temperature maps in our previous paper (Namikawa et al. 2013a, appendix), but including polarization fluctuations. We prepared the lensed CMB maps as follows.

(i) We obtain unlensed CMB temperature and polarization power spectra, $C_\ell^{\Theta\Theta}$, $C_\ell^{\Theta E}$ and C_ℓ^{EE}, with the Code for Anisotropies in the Microwave Background (CAMB; Lewis, Challinor & Lasenby 2000).

(ii) We generate Gaussian temperature fluctuations Θ_ℓ in Fourier space, based on the input power spectrum $C_\ell^{\Theta\Theta}$. Then, we also generate polarization fluctuations $E_\ell = \sqrt{C_\ell^{EE} - (C_\ell^{\Theta E})^2/C_\ell^{\Theta\Theta}}R_\ell + (C_\ell^{\Theta E}/C_\ell^{\Theta\Theta})\Theta_\ell$, where R_ℓ is the normalized Gaussian field (with zero mean and unit variance). Then, the fluctuations of Θ_ℓ and E_ℓ satisfy the input power spectra. Here, we assume that the primordial

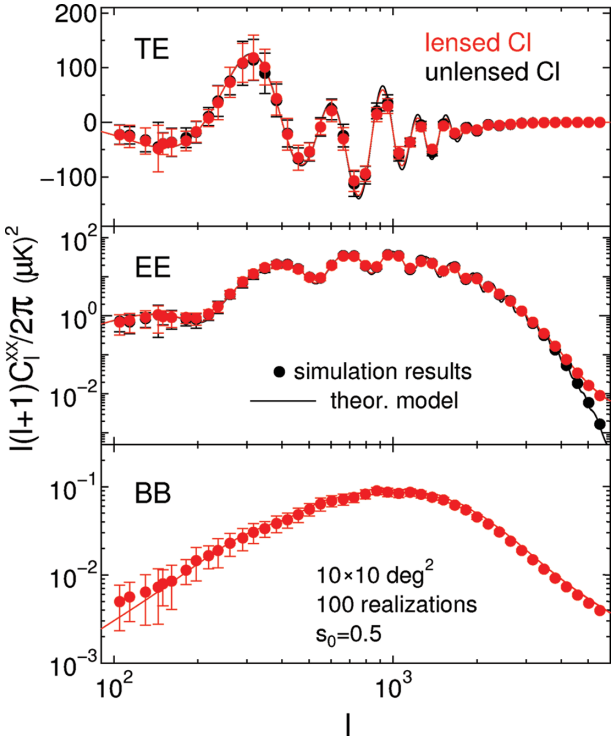

Figure B1. Lensed CMB power spectra for *TE* (upper), *EE* (middle) and *BB* (lower). The red (black) symbols are the lensed (unlensed) power spectra. The dots with error bars are our simulation results calculated from the 100 realizations of 10×10 deg^2 maps. The solid curves are the theoretical predictions of CAMB.

B-mode is zero. By performing a Fourier transform on the fluctuations (Θ_ℓ and E_ℓ), we generate an unlensed CMB map. The map is a square of $\sqrt{4\pi}$ rad ($\simeq$203 deg) on a side. We prepare 100 such unlensed maps.

(iii) We make a lensed CMB map by remapping the unlensed map according to equation (1). Here, we perform the ray-tracing simulations to obtain the deflection angles. We used a publicly available code RAYTRIX (Hamana & Mellier 2001) that follows the multiple scattering. In the standard multiple lens plane algorithm, we divide the distance from the observer to the last scattering surface (LSS) into several equal intervals and then put lens planes in every interval. The light rays emitted from the observer are deflected in every lens plane before reaching the LSS. We numerically solve the light-ray positions by solving the multilens equation and we finally obtain the angular position shifts on the LSS [see Namikawa et al. (2013), Appendix A, for a detailed discussion]. We have checked that the power spectrum of the lensing potential agrees with the expectation from CAMB.

(iv) By repeating procedures (i)–(iii), we prepared 100 lensed CMB maps. Each map has an area of 10×10 deg^2 with 1024×1024 grids, and hence the resulting angular resolution is 10 deg/1024 $\simeq$ 0.6 arcmin. Note that, in our analysis of lensing reconstruction, we further cut the maps into 5×5 deg^2.

Fig. B1 shows the CMB power spectra calculated from the 100 lensed CMB maps. The upper, middle and lower panels are for the *TE*, *EE* and *BB* power spectra, respectively. The dots with error bars are the mean and the dispersion calculated from the 100 realizations. We use $s_0 = 0.5$ for the apodization given in equation (43). Note that, in order to mitigate the effect of $E - B$ mixing due to the survey boundary effect, we estimate the lensed E and B modes using pure E and B estimators (Smith & Zaldarriaga 2007). The red (black) symbols are the results for the lensed (unlensed) case. The solid curves are the theoretical predictions of CAMB. Our simulation results agree with the theoretical prediction very well.

This paper has been typeset from a TEX/LATEX file prepared by the author.